Structure and Stability of Rhodium Clusters in NaY Studied by NMR and FTIR

Ling-Fen Rao,[†,‡] M. Pruski,*[,†] and T. S. King[†,‡]

Ames Laboratory, Department of Chemical Engineering, Iowa State University, Ames, Iowa 50011-2230

Received: March 18, 1997; In Final Form: May 20, 1997[⊗]

Small Rh clusters in NaY zeolite (Rh_c/NaY) produced by oxidation and subsequent reduction of $Rh_6(CO)_{16}$/NaY were studied by NMR, in situ FTIR, and volumetric adsorption of CO and H_2. Hydrogen uptake on bare Rh clusters measured via ^{1}H NMR was 1.0(±0.2) hydrogen per rhodium (H/Rh), while the amount of CO determined volumetrically was 2.56(±0.1) CO/Rh. These values are consistent with very high Rh dispersion. Dosing of the Rh clusters with sufficient CO regenerated $Rh_6(CO)_{16}$. The catalyst was stable to further oxidation−reduction−CO adsorption treatment cycles. Two resonance peaks were observed in the ^{1}H NMR spectra of reduced Rh_c/NaY in the presence of H_2: (i) a resonance at about 2 ppm due to hydrogen associated with the support and (ii) a broader upfield peak assigned to hydrogen adsorbed on Rh clusters. The NMR properties of hydrogen adsorbed on Rh clusters differed considerably from those observed for hydrogen on metallic Rh particles, e.g., particles produced by impregnation on NaY zeolite [Rh(imp)/NaY]. First, the intrinsic shift of the hydrogen adsorbed on Rh clusters was over 100 ppm further upfield than hydrogen adsorbed on catalysts with Rh particles larger than 2 nm. It is suggested that this increased shift reveals the paramagnetic character of Rh clusters. Second, the temperature dependence of this intrinsic shift indicated antiferromagnetic electron spin coupling. In contrast, the NMR shift of hydrogen adsorbed on Rh(imp)/NaY was nearly constant in the same temperature range (∼300−500 K). Finally, the second moment analysis showed that hydrogen was rigidly adsorbed on Rh clusters but was mobile on the surface of larger Rh particles. At a hydrogen coverage of 0.65 H/Rh, two hydrogen states on Rh clusters were indicated by this analysis and were proposed to be hydrogen adsorbed at face-bridging sites and edge-bridging sites.

1. Introduction

Transition metal clusters trapped in zeolite cages have attracted broad scientific interest and the extensive body of published work has been reviewed recently.[1,2] For example, it has been reported that hexarhodium carbonyl clusters, $Rh_6(CO)_{16}$, can be synthesized in the cages of NaY zeolite.[3−7] Studies using FTIR,[3−7] EXAFS,[6] and ^{13}C NMR[7] revealed that the rhodium carbonyl clusters are accommodated inside the supercages of NaY zeolite. They exhibit narrower and more symmetric C−O vibration IR bands[3−7] and ^{13}C NMR resonance peaks[7] compared to CO adsorbed on large Rh particles prepared by conventional impregnation methods. In this paper the term large particles refers to particles with diameters ≥2 nm and containing from a few hundred to tens of thousands of atoms. The well-defined structure of $Rh_6(CO)_{16}$/NaY presents the possibility that Rh clusters having uniform and ultrafine size can be obtained by removing the carbonyl ligands. The resulting clusters, if they are stable and reproducible, may provide a rich opportunity for a systematic study of catalytic processes on Rh.

The objective of this work was to produce highly dispersed Rh trapped in NaY using $Rh_6(CO)_{16}$/NaY as the precursor. Furthermore, we endeavored to use in situ ^{1}H NMR, ^{13}C MAS NMR, in situ FTIR, and standard selective chemisorption methods in a complementary fashion to characterize the carbonyl precursor and the Rh cluster catalyst as it experienced oxidation, reduction to form the bare Rh clusters, and CO adsorption to regenerate $Rh_6(CO)_{16}$. A major focus of this study was to probe the stability of the cluster and its size under various conditions needed to produce a working catalyst. Two important questions regarding the catalyst stability are (i) do the Rh clusters migrate out of the zeolite supercages and form larger Rh particles in the oxidation/reduction step as reported for Ru/NaY[8] and for $Rh(NH_3)_5Cl$/NaY[9,10] and (ii) does the exposure of bare Rh particles to CO induce fragmentation of the Rh as is observed with silica and alumina-supported Rh catalysts?[11,12] Another objective of this study was to determine how hydrogen adsorbed on and interacted with the bare Rh clusters.

The usefulness of solid-state NMR for this study stems from its ability to distinguish and quantify H and CO adsorbed on the metal and to probe both the geometrical arrangement[13−15] and the dynamics of adsorbed species.[16,17] Some of the traditional methods that are commonly used to characterize surface phenomena on supported metals are not easily applied to cluster catalysts. For example, dispersion determinations using H_2 in a selective chemisorption experiment are complicated by the difficulty in distinguishing hydrogen adsorbed on metal atoms from hydrogen that spills over to the support.[18] Similar experiments employing CO as an adsorbate suffer from possible CO-induced particle fragmentation[11,12] and from multiplicity of CO adsorption on highly dispersed rhodium.[19]

In this paper we present ^{13}C NMR and FTIR evidence for the well-defined structure of $Rh_6(CO)_{16}$ clusters trapped in the zeolite supercages (section 3.1). It is further demonstrated that these hexarhodium clusters can be subjected to a mild oxidation followed by a reduction treatment to produce highly dispersed, bare rhodium clusters. The bare Rh clusters can accommodate a large amount of adsorbates and can be converted back to the hexarhodium carbonyls by readsorption of CO (sections 3.2, 3.3, and 4.1). ^{1}H NMR was exploited to probe the electronic nature and physical structure of the H/Rh_c system (sections 3.4 and 4.2). It was noted via ^{1}H NMR that the H/Rh_c system exhibited a paramagnetic shift with an antiferromagnetic temperature dependence. The results presented here indicate that

* To whom correspondence should be addressed.
† Ames Laboratory.
‡ Department of Chemical Engineering.
⊗ Abstract published in *Advance ACS Abstracts,* June 15, 1997.

S1089-5647(97)00971-1 CCC: $14.00

sub-nanometer Rh clusters containing approximately six Rh atoms were produced and that these clusters were stable under the conditions investigated.

2. Experimental Section

2.1. Sample Preparation. $Rh_6(CO)_{16}$/NaY was synthesized by heating a Rh^{3+} ion-exchanged NaY zeolite (Aldrich LYZ-52) in a flowing mixture of carbon monoxide and hydrogen (2:1) at 358 K for 12 h. $Rh_6(^{13}CO)_{16}$/NaY was prepared by heating $Rh_6(CO)_{16}$/NaY at 393 K in ^{13}CO gas (98% enriched) purchased from Cambridge Isotope Laboratory. Rh loadings of 4 or 6 wt % were used in these samples. A more detailed synthesis procedure was reported elsewhere.[6,7] The formation of $Rh_6(CO)_{16}$ was confirmed by FTIR and ^{13}C MAS NMR.

Rhodium cluster catalysts (Rh_c/NaY) were prepared by oxidation of $Rh_6(CO)_{16}$/NaY in 1 atm O_2 in a temperature range 473−523 K for 2 h to remove the carbonyl ligands followed by reduction in 1 atm H_2 at 470 to 670 K for 2 h. H_2 gas was purified by passing over an Engelhard Deoxo Pd catalyst and a 5 Å molecule sieve. O_2 and CO gases (99.99%) were used without further purification.

A conventional supported catalyst [Rh(imp)/NaY] was prepared by incipient wetness impregnation of NaY zeolite with an aqueous solution of $RhCl_3$.[20] The zeolite was used to eliminate the possibility of variable support effects. The resulting wet paste was dried in air at 300 K for 24 h and at 383 K for 4 h. This catalyst (2.6 wt % Rh) was heated in static O_2 at 737 K and reduced in 1 atm H_2 at 673 K for 2 h. After reduction, the samples were evacuated at the reduction temperature for 1.5 h before measurements of IR, volumetric chemisorption, and NMR.

2.2. IR Spectroscopy. IR spectra were recorded with a Nicolet Magna 550 single-beam spectrometer equipped with an MCT detector. Each spectrum resulted from 36 scans collected at 2 cm^{-1} resolution. An ultrahigh vacuum, in situ IR cell capable of being heated to 800 K was designed and constructed for this experiment. The cell was made of stainless steel, and its background pressure after baking was less than 10^{-7} Torr. The sample was either pressed into a self-supported wafer or pressed onto a tungsten grid and placed in the Pyrex sample holder located inside the cell.

2.3. Volumetric Adsorption Isotherms. Volumetric adsorption isotherms of Rh_c/NaY were measured at 300 K in a grease-free, glass vacuum system equipped with a Pfeiffer Balzers turbomolecular pump. About 0.5 g $Rh_6(CO)_{16}$/NaY was charged and Rh_c/NaY was prepared in situ at a reduction temperature of 473 K. The first H_2 adsorption isotherm was determined in the pressure range 0.5−400 Torr. The time for equilibration at each pressure was about 40 min. The sample was then evacuated for 1 h at 4×10^{-6} Torr, and a second adsorption isotherm was determined in the same manner. CO adsorption isotherms were measured using a similar procedure.

2.4. NMR Spectroscopy. In situ ^1H NMR experiments were carried out at a ^1H resonance frequency of 250 MHz using a home-built spectrometer and a home-built probe capable of operating at variable temperatures and pressures. Approximately 0.2 g of $Rh_6(CO)_{16}$/NaY was placed in the sample tube of the NMR probe that was connected by a flexible Cajon bellow to a grease-free vacuum/gas system. The sample was oxidized and reduced in situ under the conditions described in section 2.1 to produce Rh_c/NaY. H_2 gas was dosed onto the Rh_c/NaY at the desired temperature and pressure prior to the acquisition of the NMR spectra. A similar amount of the reduced Rh(imp)/NaY was charged into an NMR tube and was rereduced in situ at 673 K. Free induction decays were acquired using a single pulse sequence with spin temperature inversion. The dwell time was 2 μs and the signal was acquired after a delay of 3 μs. Spin-echo measurements were performed using the $90_x-\tau-180_y-\tau$ sequence.

Another home-built spectrometer operating at 25.16 MHz for ^{13}C was used to measure ^{13}C NMR spectra of $Rh_6(^{13}CO)_{16}$/NaY. The probe used in this study allowed for magic angle spinning (MAS) of samples sealed in 5 mm NMR tubes.[21] The ^{13}C MAS spectra were acquired using a spin-echo sequence with the refocusing time corresponding to one rotor period.

The ^1H and ^{13}C resonance shifts are reported using the δ scale relative to tetramethylsilane (TMS) with negative values being upfield.

TABLE 1: IR Frequencies for Rh Carbonyl Species

species	IR bands[a] (cm^{-1})	ref
$Rh^+(CO)_2(O_z)_2$/NaY	2098, 2022	5, 22
$Rh^+(CO)_2(O_zH)_2$/NaY	2114, 2048	5, 22
$Rh_6(CO)_{12}(\mu_3\text{-}CO)_4$/NaY	2098s, 2066w, 1764s	3−7
$Rh_6(CO)_{12}(\mu_2\text{-}CO)_4$/NaY	2092s, 2072w, 1830s	6
$Rh_6(CO)_{16}$ (Nujol)	2078, 1800	23

[a] s and w denote strong and weak bands, respectively.

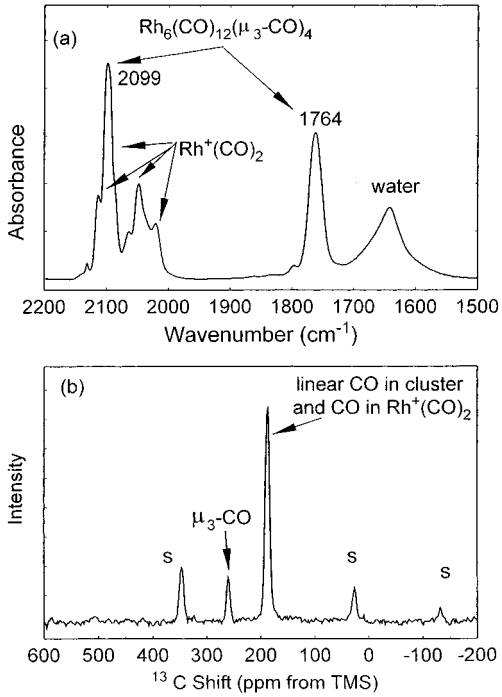

Figure 1. (a) Room temperature IR spectrum of the synthesized $Rh_6(CO)_{16}$/NaY (4 wt % Rh) after evacuation at 353 K. (b) ^{13}C MAS NMR spectrum of $Rh_6(^{13}CO)_{16}$/NaY (6 wt % Rh) under magic angle spinning at 4 kHz.

3. Results

3.1. Characterization of $Rh_6(CO)_{16}$/NaY by FTIR and ^{13}C MAS NMR. Detailed FTIR and ^{13}C MAS NMR studies of the structure of $Rh_6(CO)_{16}$/NaY were reported previously.[6,7] To facilitate the interpretation of spectroscopic data presented in this work for Rh_c/NaY and Rh(imp)/NaY, we first briefly summarize these earlier results.

Typical IR and ^{13}C MAS NMR spectra of a $Rh_6(CO)_{16}$/NaY sample are shown in parts a and b of Figure 1, respectively. Only two Rh species, $Rh_6(CO)_{16}$ and $Rh^+(CO)_2$, were observed. The assignments are consistent with previously determined IR bands summarized in Table 1.[3−7,22,23] The ^{13}C MAS NMR spectrum of $Rh_6(CO)_{16}$/NaY (Figure 1b) shows two isotropic peaks at 178 and 253 ppm representing terminal and bridging

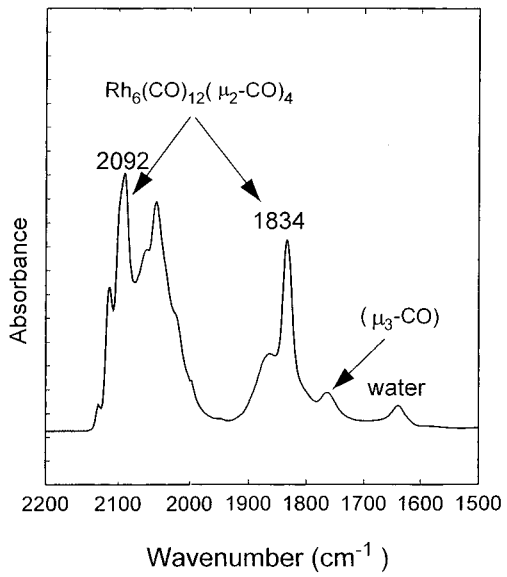

Figure 2. IR spectrum of Rh_c/NaY after exposure to 600 Torr CO at 300 K and subsequent evacuation. Background spectrum of Rh_c/NaY prior to CO adsorption was subtracted.

carbonyls, respectively. Although the linear CO in $Rh_6(CO)_{16}$ and $Rh^+(CO)_2$ are not directly resolved via the isotropic shift, the NMR spin−lattice relaxation times T_1 of these two terminal groups differed by 2 orders of magnitude, which allowed for their quantitative determination. The quantitative analysis yielded the Rh_6:Rh^+ ratio of 3:1 for a 4 wt % Rh sample and 1:1 for a 6 wt % Rh sample.[7] The intensity ratio of the linear CO to the bridging CO in the rhodium clusters was found to be 2.9(±0.2):1, in good agreement with the stoichiometry of the cluster molecule.

We note that both IR and NMR data show relatively narrow spectra. For example, the μ_3-CO band at 1764 cm^{-1} is symmetric and its line width is about $^1/_5$ of that of μ_2-CO adsorbed on Rh/SiO_2[24] or Rh/Al_2O_3.[25] Similarly, the ^{13}C NMR line widths of CO in $Rh_6(CO)_{12}(\mu_3\text{-}CO)_4$ are much narrower than those observed on Rh/SiO_2 by Duncan et al.[26] These findings show that CO ligands in $Rh_6(CO)_{12}(\mu_3\text{-}CO)_4$ are located in a uniform chemical environment in the zeolite supercages. We also note that the IR mode of the μ_3-CO is shifted by 40 cm^{-1} toward lower frequency and that the ^{13}C NMR resonance of the μ_3-^{13}CO is at about 20 ppm downfield from the one observed for $Rh_6(CO)_{16}$ in solid state[23] and in solution.[27] These shifts suggest that the tetrahedral $Rh_6(CO)_{16}$ clusters are located in the center of the supercages such that the four μ_3-CO ligands interact with four site-II Na^+ cations, which are also known to be tetrahedrally arranged.[28] Such a scenario further implies that the lone pair electrons of the oxygen ends are pulled toward the cations and the bonding electrons move toward the oxygen atom causing the observed red shift of the C−O bond vibration band observed by IR and the deshielding effect observed by NMR.

3.2. FTIR Characterization of CO Adsorption on Rh_c/NaY. The IR spectrum shown in Figure 2 was recorded following exposure of Rh_c/NaY (reduced at 470 K) to 600 Torr CO and subsequent evacuation at 300 K. Comparable spectra were acquired for several reduction temperatures values ranging from 430 to 630 K. In addition to the previously observed bands featuring CO in $Rh^+(CO)_2$ and $Rh_6(CO)_{12}(\mu_3\text{-}CO)_4$ we observed two bands at 2092 and 1834 cm^{-1}. Based on our previous work,[6] we assign these bands to the linear and the edge-bridging CO in $Rh_6(CO)_{12}(\mu_2\text{-}CO)_4$. The full width at half-maximum (fwhm) of the 2092 and 1834 cm^{-1} bands was 12 and 18 cm^{-1}, which is considerably less than the fwhm of linear and bridging CO (17 cm^{-1} and 80−90 cm^{-1}, respectively) on Rh/SiO_2 and Rh/Al_2O_3 catalysts.[24,25] Again, these results suggest that the CO ligands on Rh_c/NaY experience relatively homogeneous chemical environments. We noticed that at room temperature all $Rh_6(CO)_{12}(\mu_2\text{-}CO)_4$ species converted to $Rh_6(CO)_{12}(\mu_3\text{-}CO)_4$ upon addition of hydrogen or deuterium.

TABLE 2: Hydrogen and Carbon Monoxide Uptake by Rh_c/NaY and Rh(imp)/NaY Determined Volumetrically and by NMR Spectroscopy

	Volumetric[a]					
	H/Rh			CO/Rh		
	total	weak	strong	total	weak	strong
Rh_c/NaY, 2 wt %, 473 K red, 300 K ads	1.4	0.6	0.8	2.7	0.1	2.6
Rh_c/NaY, 4 wt %, 473 K red, 300 K ads	1.4	0.6	0.8	2.9	0.3	2.6
CO(2.5)−Rh_c/NaY, 4 wt %, CO saturated, 300 K ads	0.0	0.0	0.0			

	^1H NMR[b]		
	total	H/sup	H/Rh
Rh_c/NaY, 4 wt %, 673 K red, 370 K ads	1.3	0.2	1.0
Rh_c/NaY, 6 wt %			
673 K red, 300 K ads	1.5	0.4	1.1
673 K red, 410 K ads			1.0
Rh(imp)/NaY, 2.6 wt %			
673 K red, 300 K ads			0.38
673 K red, 373 K ads			0.28

[a] Experimental error is ±0.05. [b] Experimental error is ±0.20.

3.3. Adsorption Isotherms. Hydrogen and CO uptakes on Rh_c/NaY determined by volumetric adsorption and NMR spectroscopy are given in Table 2. The H/Rh and CO/Rh values give the number of adsorbed hydrogen atoms and CO molecules per Rh atom in the sample. The total weak and strong hydrogen uptakes were determined by the standard volumetric procedure (extrapolation of the linear high-pressure parts of the first and second isotherms to zero pressure and taking the difference) and were found to be approximately 1.4, 0.6, and 0.8 H/Rh, respectively. The results of quantitative ^1H NMR (see section 3.4 and ref 29 for more detail) indicated that the hydrogen associated with Rh in Rh_c/NaY saturated at 1.0(±0.2) H/Rh. The amount of strongly adsorbed CO was 2.6 CO/Rh, close to the stoichiometric ratio in $Rh_6(CO)_{16}$, which substantiates the existence of multicarbonyl adsorption and is in agreement with FTIR. Note that no hydrogen uptake was observed for the sample that was saturated with CO. The hydrogen adsorption on Rh(imp)/NaY measured by ^1H NMR yielded 0.38 H/Rh, indicating a Rh dispersion of 38%.

3.4. ^1H NMR Spectra of Rh_c/NaY and Rh(imp)/NaY in the Presence of Hydrogen. *3.4.1. Pressure and Temperature Dependence of the ^1H Shift.* ^1H NMR spectra of Rh_c/NaY (4 wt % Rh) taken at 370 K under various H_2 pressures are shown in Figure 3. For clarity, the ranges 200 to 100 ppm and −50 to −400 ppm are shown separately using different intensity scales. After reduction and subsequent evacuation at 673 K, Rh_c/NaY exhibited a single, 7 kHz wide (fwhm) ^1H resonance at 2 ppm [see spectrum a], which represents primarily OH groups within the zeolite framework.[30,31] The spectrum changed significantly after exposure to H_2 gas. A new peak, marked c-H, associated with the hydrogen adsorbed on Rh clusters, appeared in the upfield portion of the spectrum. As the H_2 pressure increased from 2 to 804 Torr [see spectra b−f], the c-H peak shifted from −255 to −155 ppm and its line width narrowed from ∼20 kHz to ∼14 kHz. A set of spectra with essentially the same line shape parameters were observed for

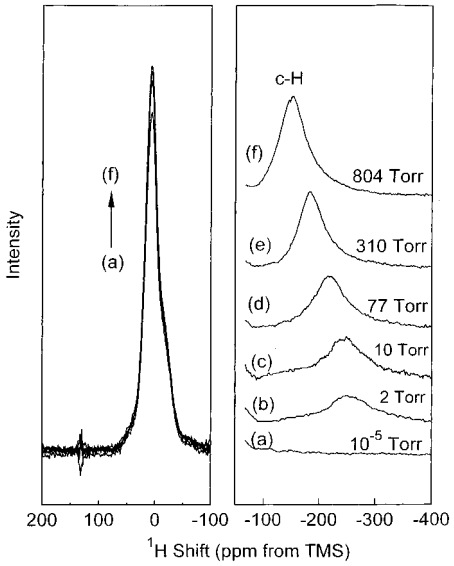

Figure 3. In situ ^{1}H NMR spectra of Rh_c/NaY at 370 K in the range 200 to −100 ppm and −50 to −400 ppm: (a) after reduction and evacuation to 4×10^{-6} Torr at 673 K; (b) following exposure to H_2 gas at 2 Torr; (c) 10 Torr; (d) 77 Torr; (e) 310 Torr; (f) 804 Torr. A 60 s delay between scans was used to avoid the saturation of downfield resonance.

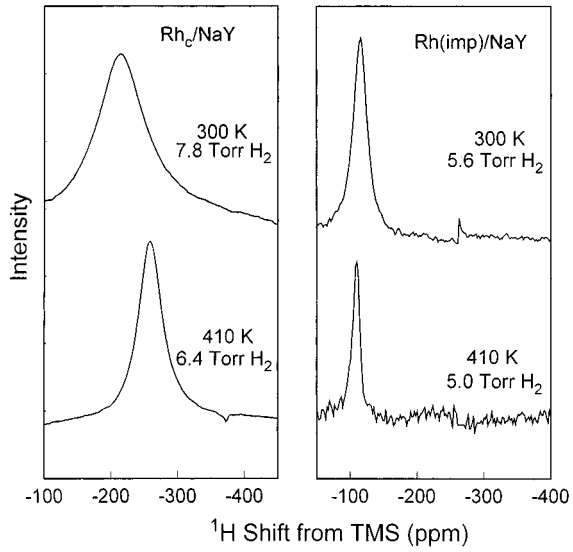

Figure 4. In situ ^{1}H NMR spectra of hydrogen adsorbed on Rh_c/NaY (6 wt % Rh) and on Rh(imp)/NaY at 300 and 410 K.

the Rh_c/NaY with 6 wt % Rh. We note that although the intensity of c-H steadily increased with pressure, the amount of hydrogen adsorbed on the metal saturated at approximately 1.0 H/Rh. The increasing intensity results mostly from exchange between hydrogen on the metal and H_2 gas, which will be described in detail elsewhere.[29]

The ^{1}H NMR spectra of Rh(imp)/NaY also showed two resonances, with the peak representing hydrogen on rhodium located less upfield (e.g., about −116 ppm at 370 K and 5 Torr of hydrogen). The pressure dependence of this resonance (not shown) is similar to Rh_c/NaY and is also consistent with that observed previously on Rh/TiO_2[32−34] and $Rh/SrTiO_3$ catalysts.[35,36]

^{1}H NMR spectra of hydrogen adsorbed on Rh_c/NaY (6 wt % Rh) and Rh(imp)/NaY at 300 and 410 K are shown in Figure 4. A plot of intrinsic ^{1}H NMR shifts (see section 4.2.1) of hydrogen on the two samples versus $1/T$ is given in Figure 5. The intrinsic shift of the c-H resonance moved upfield with

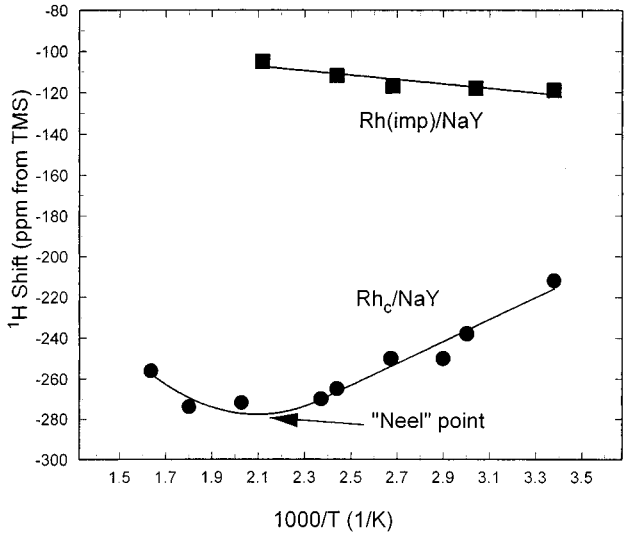

Figure 5. Temperature dependence of the intrinsic ^{1}H NMR shift for H/Rh in (a) Rh(imp)/NaY and (b) Rh_c/NaY. At temperatures above 650 K for the Rh_c/NaY and 473 K for the Rh(imp)/NaY, the peak intensities were too small to be accurately measured.

increasing temperature up to 485(±25) K, beyond which the change of shift reversed. In contrast, the hydrogen adsorbed on Rh(imp)/NaY exhibited a very slight upfield change of shift when temperature was increased from 298 to 470 K.

3.4.2. $^1H-^1H$ Dipolar Interaction of Adsorbed Hydrogen. The results of the previous section demonstrated that both the magnitude and the temperature dependence of ^{1}H shifts on Rh_c/NaY were different from those on larger Rh particles in Rh(imp)/NaY. It also appeared that the line broadening mechanisms differed between these two samples. For example, at a coverage of 0.65 the c-H peak measured at room temperature using single pulse excitation was a single Gaussian line of 42-(±3) kHz fwhm. Under the same conditions, hydrogen adsorbed on Rh(imp)/NaY yielded a Lorentzian line with a fwhm of only 6.8 kHz.

The overall line broadening includes contributions from homo- and heteronuclear dipolar coupling ($^1H-^1H$ and $^1H-^{103}Rh$, respectively), the exchange processes, the susceptibility effects, and the heterogeneity of adsorption sites. The contribution of homonuclear dipolar coupling can be assessed by the analysis of the second moment measured from the spin-echo decay $A(\tau)$ after a $\pi/2-\tau-\pi-\tau$ sequence.[37] This decay can be used to determine the homonuclear second moment M_2^{HH} or the relaxation time T_2^{HH} using the equations

$$A(2\tau) = A(0)\exp\left\{-\frac{M_2^{HH}(2\tau)^2}{2}\right\} \quad (1)$$

and

$$A(2\tau) = A(0)\exp\left\{-\frac{2\tau}{T_2^{HH}}\right\} \quad (2)$$

for the Gaussian and Lorentzian lines, respectively.

The experimental data obtained for Rh_c/NaY and Rh(imp)/NaY at a 0.65 coverage are summarized in Table 3. For the c-H resonance, the spin-echo decay is described by a superposition of two Gaussian functions with second moments of 2.0×10^8 and 7.4×10^6 Hz^2, corresponding to (at least) two states of adsorbed hydrogen denoted by "a" and "b". The dipole−dipole interaction between hydrogens contributed ∼33 kHz to the observed total line width of ∼42 kHz. The Rh(imp)/NaY sample also revealed the presence of two components of the

TABLE 3: Second Moment M_2^{HH}, Spin−Spin Relaxation Time T_2^{HH}, and the Full Width at Half Maximum (fwhm) Contributed from H−H Dipole−Dipole Interaction Determined by Spin-Echo Method[a]

		component "a"			component "b"			
adsorbate/sample	$fwhm_{total}$ (kHz)	M_{2a}^{HH} (Hz^2)	T_{2a}^{HH} (μs)	$fwhm_a$ (kHz)	M_{2b}^{HH} (Hz^2)	T_{2b}^{HH} (μs)	$fwhm_b$ (kHz)	N_a/N_b
$H_2/Rh_c/NaY$	44	2.0×10^8 (G)	16	33	7.4×10^6 (G)	83	6.4	$3.3 \pm .5$
$H_2 + D_2/Rh_c/NaY$ (H/D = 1/9)	37	2.1×10^7 (G)	49	11	6.6×10^5 (G)	280	2.6	$2.6 \pm .5$
H_2/Rh(imp)/NaY	6.8	5.2×10^6 (G)	99	3.2	1.7×10^5 (G)	540	0.59	1.0
		1.4×10^7 (L)	60	5.3	2.9×10^5 (L)	420	0.77	0.79

[a] G and L denote Gaussian and Lorentzian fits, respectively.

TABLE 4: ^{1}H NMR Resonance Shifts of Rh Hydride Complexes and of Hydrogen Adsorbed on Supported Rh Catalysts

sample	Rh dispersion, % (particle size)	shift, ppm	fwhm, kHz	ref
$[Rh_{13}(CO)_{24}H]^{4-}$		−25.5 (300 K)		39
$[Rh_{13}(CO)_{25}H_2]^{3-}$		−26.7 (300 K)		39
$[Rh_{13}(CO)_{24}H_3]^{2-}$		−29.3 (300 K)		39
$[Rh_{13}(CO)_{24}H_4]^{-}$		−31.2 (300 K)		39
$[Rh_{14}(CO)_{25}H]^{3-}$		−31.4 (193 K)		39
Rh/TiO_2	15 (6 nm)	−125 (300 K)	2.8	33, 34
$Rh/SrTiO_3$	15 (6 nm)	−140 (300 K)	2.8	35, 36
Rh/SiO_2		−104 (300 K, 1 Torr)	2.2	40
Rh/SiO_2	50 (2 nm)	−140 (300 K, 6 Torr)		41
Rh/Al_2O_3	50 (2 nm)	−135 (300 K, 6 Torr)	5.0	42
Rh/NaY (3 wt %)	38	−119 (300 K, 5 Torr)	6.8	this work
		−116 (410 K, 5 Torr)	3.	this work
Rh_c/NaY (4 wt %)	>85 (<1 nm)	−270 (370 K, 0.2 Torr)	20.	this work
Rh_c/NaY (6 wt %)	>85 (<1 nm)	−230 (300 K, 10^{-5} Torr)	41.	this work
		−215 (300 K, 6 Torr)	24.	this work
		−263 (410 K, 1 Torr)	7.0	this work

spin-echo decay. However, the observed second moments were much smaller than those on Rh_c/NaY with the same coverage. For most conditions used in our study, the echo decay in the Rh(imp)/NaY sample could be better fit using a Lorentzian function.

4. Discussion

Ample experimental data presented above suggest that Rh_c/NaY particles produced by oxidation and subsequent reduction of $Rh_6(CO)_{16}$/NaY remain in the form of small clusters, most likely Rh_6, throughout the various stages of treatment. Other possible scenarios, which include (i) migration of rhodium out of the zeolite supercages during oxidation and/or reduction to form larger Rh particles and (ii) the fragmentation of bare Rh particles induced by adsorption of CO, are not substantiated by the results of this work. We discuss these results below.

4.1. IR Spectroscopy. The IR spectrum of Figure 2 suggests that upon exposure to CO the majority of bare Rh clusters was restored to the form of the $Rh_6(CO)_{16}$ precursor. The spectrum exhibits a relatively narrow, strong absorption band at 1834 cm^{-1}, which we assigned to the bridging groups in $Rh_6(CO)_{12}(\mu_2\text{-}CO)_4$. Upon addition of hydrogen, the $Rh_6(CO)_{12}(\mu_2\text{-}CO)_4$ species readily isomerized to the precursor, $Rh_6(CO)_{12}(\mu_3\text{-}CO)_4$. A similar interconversion has been reported earlier for $Ir_6(CO)_{12}(\mu_2\text{-}CO)_4$ and $Ir_6(CO)_{12}(\mu_3\text{-}CO)_4$ in dichloroethane solution,[38] but the mechanism is not known. Possibly, H_2 molecules collide with the Rh carbonyl clusters, just as the solvent molecules collide with the Ir carbonyl clusters, "pushing" the carbonyls into a more stable isomer. We also note that, although a comparison with the spectrum of Figure 1b shows a slight increase of the $Rh^+(CO)_2$ to $Rh_6(CO)_{16}$ intensity ratio in the Rh_c/NaY sample, the CO-induced fragmentation of Rh particles did not proceed as significantly as in Rh/Al_2O_3.[11,12]

The finding that the bare Rh clusters convert to $Rh_6(CO)_{16}$ suggests that these bare clusters are not very large, if at all different from Rh_6. If large particles were formed prior to CO adsorption, reconstruction of $Rh_6(CO)_{16}$ by reintroduction of CO would imply extensive migration of CO/Rh moieties between the supercages. This is an unlikely process that would be notably different from the formation of the original $Rh_6(CO)_{16}$ clusters via a reductive carbonylation of Rh^{3+} cations associated with the zeolite framework.

4.2. ^{1}H NMR. Although IR spectroscopy probed the Rh_c/NaY sample after readsorption of CO, ^{1}H NMR allowed for examination of Rh clusters in an almost bare state. There are several significant differences in the ^{1}H NMR spectra of hydrogen adsorbed on Rh_c/NaY compared with larger, supported Rh particles: (i) a much larger intrinsic shift, (ii) a more complex temperature dependence of this shift, and (iii) an increased line width. These differences reflect the distinct hyperfine interactions associated with the surface of supported particles compared with small Rh clusters located within the zeolite framework.

4.2.1. Intrinsic ^{1}H NMR Shift of H Adsorbed on Rh_c/NaY. The term "intrinsic shift" is used throughout this work to describe the position of the ^{1}H NMR line of adsorbed hydrogen extrapolated to zero pressure (or coverage). The strong pressure dependence in ^{1}H NMR spectra of Figure 3 is due mainly to the fast exchange between adsorbed hydrogen and H_2 gas. As a result, the NMR resonance frequency depends on the molar ratio of surface hydrogen to H_2 gas and may be affected by the experimental settings (dead volume inside the NMR tube, sample packing density, metal loading, dispersion, etc.). Also, the adsorbate/substrate interaction can be coverage dependent (see, for example, refs 35−36). The intrinsic shift provides a coverage independent measure of hydrogen−metal interactions that is not influenced by these experimental factors.

In Table 4 the ^{1}H intrinsic shifts of c-H are compared with those of hydrogen on other Rh catalysts and in rhodium hydride complexes. In general, the ^{1}H shifts for Rh hydride complexes

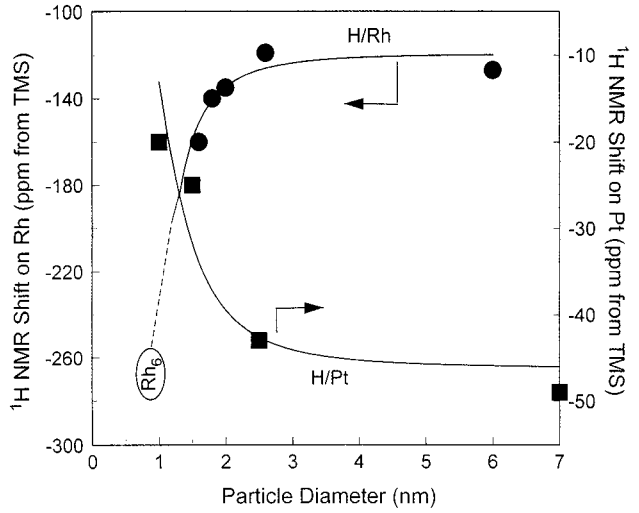

Figure 6. ^{1}H NMR shifts of hydrogen adsorbed on Rh (●) and Pt (■) versus the metal particle size (see also Table 4).

are in the range −20 to −40 ppm,[39] while the resonances of hydrogen adsorbed on low dispersion Rh are found between −100 and −140 ppm.[32−36,40−42] The NMR shifts obtained in this work for the Rh(imp)/NaY sample agree with the data for low dispersion Rh catalysts. On the other hand, the lack of such resonances in the ^{1}H spectra of hydrogen on Rh_c/NaY suggests that this sample does not contain large Rh particles. This is an important result because, as noted earlier, such migration of metal atoms out of the zeolite supercages to form larger particles on the external surface of the zeolite was detected earlier for Ru/NaY[8] and for $Rh(NH_3)_5Cl$/NaY[9] catalysts. The resonances at about −250 ppm observed here for various Rh_c/NaY samples must be attributed to hydrogen on very small rhodium clusters.

We also note that the data of Table 4 appear on a reasonably smooth curve when plotted as a function of the particle size (see Figure 6). This raises the possibility of using NMR shifts for determination of metal dispersion. However, one should proceed with caution because different mechanisms are responsible for the observed shifts in supported metals and the molecule-like clusters. In large Rh particles the electronic structure approaches the band structure of an extended lattice and yields the size independent Knight shift of about −100 ppm. The Knight shift has been attributed to the bonding overlap of the 1s orbitals of chemisorbed hydrogen with the conduction electrons of the metal.[43] Small Rh clusters, on the other hand, do not possess metallic properties. When present in the form of $Rh_6(CO)_{16}$/NaY, the clusters are coordinately saturated and, as expected, exhibit isotropic ^{13}C shifts of the terminal and bridging carbonyls that are typical of diamagnetic Rh−CO complexes.[7] Since quantitative ^{1}H NMR measurements showed that hydrogen uptake on Rh_c/NaY clusters was only 1.0(±0.2) H/Rh, these clusters are not expected to be coordinately saturated. Thus, unpaired electrons may produce strong local magnetic fields consistent with the large shifts observed in the ^{1}H NMR spectra of Figures 3 and 4. However, the interpretation of the observed spectra in terms of the cluster structure is not straightforward. Even in well characterized systems the explanation of the paramagnetic shifts is usually complex.[44,45] First, although the Rh_6 clusters are likely to be a dominant structure, other Rh_n complexes with $n \neq 6$ may be formed. Such complexes are known to have unusual magnetic properties. For example, a theoretical study predicted that the ground state of bare Rh_{13} has 21 unpaired electrons.[46] The magnetic moment of bare, gas-phase Rh_n clusters ($n = 12-32$) was measured by Cox et al.[47] who found that these clusters possessed 0.4−0.9 unpaired electrons per Rh atom and that the number of unpaired electrons decreased with increasing n. Second, it is currently unknown how the electronic properties of the Rh clusters in Rh_c/NaY are affected by chemisorbed hydrogen and by the interaction with the zeolite framework.

4.2.2. Temperature Dependence of the c-H Shift. The temperature dependence of the intrinsic shift of hydrogen on Rh_c/NaY (Figure 5) resembles the temperature dependence of the magnetic susceptibility of an antiferromagnetic material; the shift increases with temperature up to a critical point called the Neel temperature and then decreases in the normal paramagnetic fashion because of thermal randomization of spins.[44a] A potential explanation of the temperature behavior of our system is to assume antiferromagnetic spin coupling in rhodium such as observed previously in metal cluster compounds, e.g., binuclear Rh and Cu complexes, $Rh_2(CH_3CO_2)_4 \cdot 2H_2O$ and $Cu_2(CH_3CO_2)_4 \cdot 2H_2O$,[44b] as well as in two iron ferredoxines.[45b] A free Rh atom has one unpaired electron. In a small cluster there is a finite overlap of the orbitals of the Rh atoms, and according to the Pauli principle, the electron spins assume antiparallel alignment. Such spin pairing lowers the free energy of the Rh cluster system, and its effect is antiferromagnetic.[44c] At low temperatures, when thermal energy (kT) is much less than the electron exchange energy, most of the Rh clusters remain paired. As temperature increases, the clusters exhibit larger unpaired electron density, which is reflected in the NMR peak shift toward higher field. Above the Neel point the Curie behavior sets in. In this work the Neel point is around 485 K, which is over 200 K higher than in $Cu_2(CH_3CO_2)_4 \cdot 2H_2O$ and may indicate a stronger electronic coupling interaction between the Rh atoms. Figure 5 shows that the ^{1}H NMR shift of hydrogen adsorbed on Rh(imp)/NaY is almost independent of temperature, which is consistent with its interpretation as a Knight shift.[43]

4.2.3. Second Moment Analysis of ^{1}H NMR Spectra. It is known that the spin-echo sequence $^{\pi}/_2-\tau-\pi-\tau$ refocuses the interactions that are linear in I_z (e.g., chemical shift, inhomogeneity of the magnetic field, and heteronuclear dipolar coupling), whereas the homonuclear dipolar interactions, which are not refocused, are mainly responsible for the echo decay. However, the usefulness of the spin-echo for selective measurement of the homonuclear dipole−dipole couplings could be limited when $M_2^{II} > M_2^{IS}$.[37,48,49] Since the value of M_2^{HH} (i.e., the contribution of the hydrogen−hydrogen dipolar interaction to the observed ^{1}H line width) depends on the conditions used for the sample preparation and the measurements (e.g., temperature and coverage), we first tested the applicability of the spin-echo method using samples adsorbed with hydrogen heavily diluted with deuterium.

The exchange of hydrogen by deuterium on any given site reduces the contribution of that site to the second moment by a factor[50]

$$\alpha = \frac{4}{9}\frac{\gamma_D^2 I_D(I_D+1)}{\gamma_H^2 I_H(I_H+1)} = 0.0236 \qquad (3)$$

where I_H, I_D , γ_H, and γ_D denote the hydrogen and deuterium spins and magnetogyric ratios, respectively. In the case of random substitution of hydrogen with deuterium, the total proton second moment, M_2^{HH+DD}, can be written as

$$M_2^{HH+DD} = M_2^{HH}[1 - f(1-\alpha)] \qquad (4)$$

where f is the molar fraction of deuterium. For the two adsorbed states c-H_a and c-H_b at a coverage of 0.65 and by use of a 9:1

TABLE 5: Second Moments M_2^{HH} and the Corresponding Rhodium−Hydrogen Distances for Various Structural Models

model	coverage (H/Rh)	M_2^{HH} (kHz)	r_{Rh-H} (Å)
1. $Rh_6(H)_6$, 6 H in terminal positions	1.0	$1.47 \times 10^{6\,a}$	1.7[b]
2. $Rh_6H(H)_6$, 6 H in terminal positions and 1 H in the center	1.16	$5.10 \times 10^{6\,a}$	1.7[b]
3. $Rh_6H(H)_3$, 3 H randomly distributed in terminal positions and 1 in the center	0.67	$4.50 \times 10^{6\,a}$	1.7[b]
4. $Rh_6(\mu_3\text{-}H)_4$, μ_3-H at every other face	0.67	$2.0 \times 10^{8\,c}$	1.58[a]
5. $Rh_6(\mu_3\text{-}H)_4$, μ_3-H randomly distributed	0.67	$2.0\times 10^{8\,c}$	1.68[a]
6. $Rh_6(\mu_2\text{-}H)_4$, μ_2-H positioned as μ_2-CO in edge-bridging $Rh_6(CO)_{16}$	0.67	$0.35 \times 10^{6\,c}$	1.69[a]
7. 3-D H lattice, fcc, $r_{H-H} = 2.68$ Å		$1.48 \times 10^{8\,a}$	
8. 2-D H adlayer on Rh(111), $r_{H-H} = 2.68$ Å	1.0	$7.80 \times 10^{7\,a}$	
	0.65	$5.10 \times 10^{7\,a}$	

[a] Calculated. [b] Assumed values. [c] Experimental.

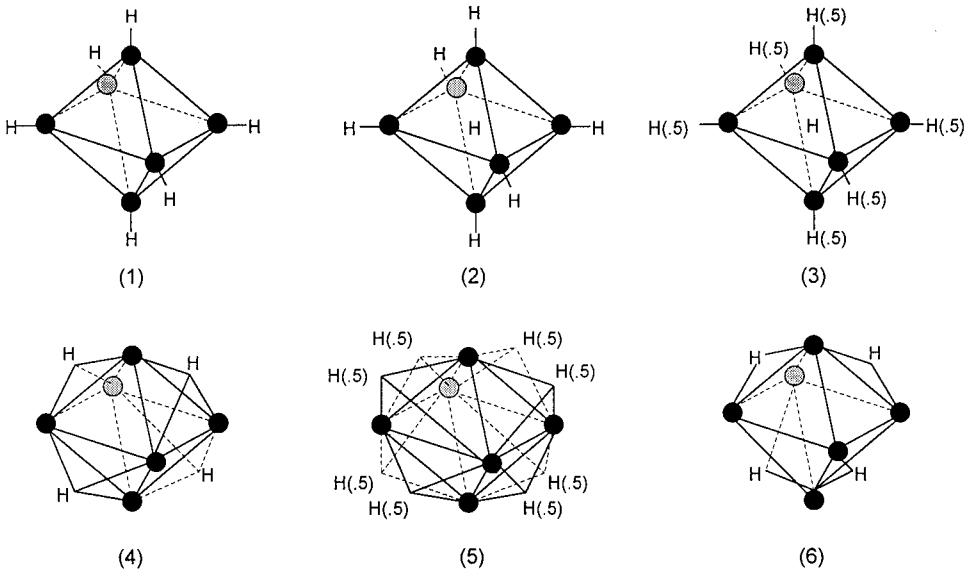

Figure 7. Structural models for hydrogen adsorption on Rh_6 clusters. Models 3 and 5 assume random distribution of hydrogen at the sites with the probability given by the number in parentheses.

mixture of D_2 and H_2, the spin-echo measurement yielded M_2^{HH+DD}/M_2^{HH} ratios of 0.10(±0.01) and 0.09(±0.01), respectively (see Table 3). This is in reasonable agreement with the value of 0.12 calculated from eq 4, which substantiates the use of the spin-echo method to investigate dipolar interactions between protons in these samples. This result and the values of the second moment reported in Table 3 indicate that hydrogen adsorbs rigidly on Rh clusters at a coverage of 0.65, and its geometrical arrangement can be probed using the formula[43]

$$M_2^{HH} = \frac{3}{5}\gamma^2\hbar I(I+1)\frac{1}{N}\sum_{i,j} r_{i,j}^{-6} \qquad (5)$$

where $r_{i,j}$ is the distance between hydrogens i and j, $\hbar$ is the Planck constant, and N is the number of hydrogen atoms occupying inequivalent positions in the repeating structural unit.

Equation 5 was used to calculate the second moments and the corresponding hydrogen−rhodium distances r_{Rh-H} for several possible structural models. These include (see Table 5 and Figure 7) models 1−3 involving terminal hydrogen and models 4−6 involving bridged hydrogen. In addition, the second moment calculations were performed for a hypothetical, three-dimensional cubic array of hydrogen (model 7) and for hydrogen adsorbed on a Rh(111) surface (model 8). The last two models will be used to explain the line shapes observed for the Rh(imp)/NaY sample.

The M_2^{HH} values listed in Table 5 need some clarification. For structures 1−3 we calculated r_{H-H} and M_2^{HH} assuming the interatomic distances $r_{Rh-H} = 1.7$ Å and $r_{Rh-Rh} = 2.7$ Å. These assumptions are based on typical metal−hydrogen bond lengths for known organometallic compounds and on earlier results of an EXAFS study of a similarly prepared Rh/NaY sample.[6] A different procedure was used for models 4−6. Since there is no relevant literature data regarding hydrogen in bridged positions, we calculated the r_{H-H} distances for these models using eq 5 and the experimental values of M_2^{HH}. The r_{Rh-H} distances were then calculated assuming, again, that $r_{Rh-Rh} = 2.7$ Å. The second moment of a three-dimensional hydrogen lattice (model 7) was calculated by Chang et al.[51] The calculations of M_2^{HH} for the two-dimensional structure (model 8) were based on the r_{H-H} values deduced from single-crystal studies assuming that hydrogen adsorbs on top of exposed Rh atoms.[52,53]

A comparison of Tables 3 and 5 indicates that at a coverage of 0.67, models 1−3 are inconsistent with the experimental M_2^{HH} values. Similarly, model 4 yields a r_{Rh-H} that is outside of the known metal−H bond length range. On the other hand, a reasonable r_{Rh-H} distance of 1.68 Å was obtained using model 5 and the experimental M_{2a}^{HH} value of 2.0×10^8 Hz^2. In this case, the hydrogen atoms are located 0.57 Å above the triangle faces. The face-bridging hydrogen model 5 is consistent with the single-crystal studies that showed that hydrogen adsorbs preferentially on 3-fold Rh sites at low coverages.[52] Similarly, the adsorbed state c-H_b with a M_{2b}^{HH} of 7.4×10^6 Hz^2 (see Table 3) is well explained assuming the presence of the edge-bridging structure (model 6). Considering the fact that H_2 gas induces transformation of an edge-bridging $Rh_6(CO)_{16}$ isomer into face-bridging isomer (see section 3.2), hydrogen may have some affinity to the edge-bridging sites. The measured c-H_a to

c-H_b ratio of about 3:1 shows that, similar to Rh carbonyl clusters, the face-bridging isomer of Rh hydride is more stable.

Our experiments showed that, in contrast to the above results for Rh_c/NaY, hydrogen exhibits increased mobility on large Rh particles in Rh(imp)/NaY. First, the observed NMR line was better fit with a Lorentzian function. Second, the line width and the second moment values observed for hydrogen adsorbed on Rh(imp)/NaY at a coverage of 0.65 are much smaller than those calculated under the same conditions for adsorption on an extended two-dimensional surface (model 8). Third, earlier ^2H studies of large Rh particles supported on Al_2O_3, SiO_2, and NaY did not reveal quadrupolar line broadening and thus suggested fast mobility of the adsorbed deuterium.[20,51] The types of motion that can be responsible for these effects include diffusion on a single metal particle without desorption from its surface and/or fast diffusion from one metal particle to another, similar to that observed in our earlier studies of Ru/SiO_2 and $RhPt/SiO_2$ catalysts.[16,17,42]

5. Conclusion

Oxidation and subsequent reduction of the well-defined $Rh_6(CO)_{16}$/NaY resulted in uniform, highly dispersed Rh clusters trapped in the zeolite supercages. These Rh clusters were reconstructed in the zeolite cages into $Rh_6(CO)_{16}$ and $Rh^+(CO)_2$ upon CO adsorption. The results that we have presented to support these conclusions include (i) FTIR spectra of adsorbed CO, which are dominated by the bands assigned to the linear and the edge-bridging CO in $Rh_6(CO)_{12}(\mu_2\text{-}CO)_4$, (ii) CO uptake consistent with the multicarbonyl adsorption of ~2.5 CO/Rh, (iii) ^1H NMR spectra of adsorbed hydrogen, which show resonances attributed to small rhodium clusters and no evidence of larger (>2 nm) particles, and (iv) the temperature dependence of the ^1H NMR shift, which may be explained as resulting from metal−metal interactions between atoms confined in an isolated cluster. Finally, the second moment analysis of ^1H NMR spectra indicated that hydrogen adsorbed on Rh_c/NaY is immobile and appears to occupy the face-bridging and edge-bridging positions in Rh_6 clusters.

Acknowledgment. This research was supported by the U.S. Department of Energy, Office of Basic Energy Science, Division of Chemical Sciences, under Contract W-7405-ENG-82 and the National Science Foundation, Engineering Research Equipment Grant CBT-8507418. Additional support was provided by the Exxon Education Foundation.

Author-Supplied Registry Numbers: Rh, 7440-16-6; H_2, 1333-74-0; CO, 630-08-0; $Rh_6(CO)_{12}(\mu_3\text{-}CO)_4$, 28407-51-4; $Rh_6(CO)_{12}(\mu_2\text{-}CO)_4$, 143006-99-9.

References and Notes

(1) Sachtler, W. M. H.; Zhang, Z. *Adv. Catal*. **1993**, *39*, 129.

(2) Ichikawa, M. *Adv. Catal*. **1992**, *38*, 283.

(3) Mantovani, E.; Palladino, N.; Zanobi, A. *J. Mol. Catal*. **1977/1978**, *3*, 285.

(4) Gelin, P.; Ben Taarit, Y.; Naccache, C. *J. Catal*. **1979**, *59*, 357.

(5) Rode, E. J.; Davis, M. E.; Hanson, B. E. *J. Catal*. **1985**, *96*, 574.

(6) Rao, L.-F.; Fukuoka, A.; Ichikawa, M. *J. Phys. Chem*. **1990**, *94*, 5317.

(7) Rao, L.-F.; Hwang, S. J.; King, T. S.; Pruski, M. *J. Phys. Chem*. **1996**, *100*, 5668.

(8) Shoemaker, R.; Apple, T. *J. Phys. Chem*. **1987**, *91*, 4024. Cho, S. J.; Jung, S. M.; Shul, Y. G.; Ryoo, R. *J. Phys. Chem*. **1992**, *96*, 9922.

(9) Bush, F.; Jaeger, N. I.; Schulz-Ekloff, G.; Schell, R.; Klein, H.; Fuess, H. *Zeolites* **1996**, *17*, 244.

(10) Tonscheidt, A.; Ryder, P. L.; Jaeger, N. I.; Schulz-Ekloff, G. *Zeolites* **1996**, *16*, 271.

(11) Van't Blik, H. F. T.; Van Zon, J. B. A. D.; Huizinga, T.; Vis, J. C.; Koningsberger, D. C.; Prins, R. *J. Am. Chem. Soc*. **1985**, *107*, 3139.

(12) Basu, P.; Panayotov, D.; Yates, J. T., Jr. *J. Phys. Chem*. **1987**, *91*, 3133.

(13) DeMenorval, L. C.; Fraissard, J. P. *Chem. Phys. Lett*. **1981**, *77*, 309.

(14) Neinecke, N.; Haul, R. *Ber. Bunsen-Ges. Phys. Chem*. **1984**, *88*, 1232.

(15) Chang, T.-H.; Cheng, C.-P.; Yeh, C.-T. *J. Catal*. **1992**, *138*, 457.

(16) Engelke, F.; Vincent, R.; King, T. S.; Pruski, M. *J. Chem. Phys*. **1994**, *101*, 7262.

(17) Engelke, F.; Bhatia, S.; King, T. S.; Pruski, M. *Phys. Rev. B*. **1994**, *49*, 2730.

(18) Kip, B. J.; Duivenvoorden, F. B. M.; Koningsberger, D. C.; Prins, R. *J. Catal*. **1987**, *105*, 26.

(19) Wong, T. T. T.; Stakheev, A. Y.; Sachtler, W. M. H. *J. Phys. Chem*. **1992**, *96*, 7733.

(20) Chang, T.-H.; Cheng, C.-P.; Yeh, C.-T. *J. Phys. Chem*. **1992**, *96*, 4151.

(21) Pruski, M.; Sanders, D. K.; King, T. S.; Gerstein, B. C. *J. Magn. Reson*. **1992,** *96*, 574.

(22) Shannon, R. D.; Vedrine, J. C.; Naccache, C.; Lefebvre, F. *J. Catal*. **1984,** *88*, 431.

(23) *The Aldrich Library of FTIR Spectra*; Pouchert, C. J., Ed.; Aldrich: Milwaukee, WI, 1985; p 1300.

(24) Srinivas, G.; Chuang, S. S. C. *J. Catal*. **1993**, *144*, 131.

(25) Yates, J. T., Jr.; Duncan, T. M.; Worley, S. D.; Vaughn, R. W. *J. Chem. Phys*. **1979**, *70*, 1219.

(26) Duncan, T. M.; Zilm, K. W.; Hamilton, D. M.; Root, T. W. *J. Phys. Chem*. **1989**, *93*, 2583.

(27) Heaton, B. T.; Towl, A. D. C. *J. Chem. Soc., Chem. Commun*. **1975**, 523.

(28) Jelinek, R.; Ozkar, S.; Ozin, G. A. *J. Phys. Chem*. **1992**, *96*, 5949.

(29) Rao, L.-F.; King, T. S.; Pruski, M. To be published.

(30) Hunger, M.; Freude, D.; Pfeifer, H. *J. Chem. Soc., Faraday Trans*. **1991**, *87*, 657.

(31) Pfeifer, H.; Freude, D.; Hunger, M. *Zeolites* **1985**, *5*, 274.

(32) Apple, T. M.; Gajardo, P.; Dybowski, C. *J. Catal*. **1981**, *68*, 103.

(33) Sanz, J.; Rojo, J. M. *J. Phys. Chem*. **1985**, *89*, 4974.

(34) Conesa, J. C.; Malet, P.; Munuera, G.; Sanz, J.; Soria, J. *J. Phys. Chem*. **1984**, *88*, 2986.

(35) Rojo, J. M.; Belzunegui, J. P.; Sanz, J.; Guil, J. M. *J. Phys. Chem*. **1994**, *98*, 13631.

(36) Sanz, J.; Rojo, J. M.; Malet, P.; Munuera, G.; Blasco, M. T.; Conesa, J. C.; Soria, J. *J. Phys. Chem*. **1985**, *89*, 5427.

(37) Boden, N.; Gibb, M.; Levine, Y. K.; Mortimer, M. *J. Magn. Reson*. **1974**, *16*, 471.

(38) Roberto, D.; Garlaschelli, L.; Pizzotti, M. *Inorg. Chem*. **1995**, *34*, 3555.

(39) Allevi, C.; Heaton, B. T.; Seregni, C.; Strona, L. *J. Chem. Soc., Dalton Trans*. **1986**, 1375.

(40) Root, T. W.; Duncan, T. M. *Chem. Phys. Lett*. **1987**, *137*, 57.

(41) Sheng, T. C.; Gay, I. D. *J. Catal*. **1982**, *77*, 53.

(42) Savargaonkar, N.; Khanra, B. C.; Pruski, M.; King, T. S. *J. Catal*. **1996**, *162*, 277.

(43) Slichter, C. P. *Principles of Magnetic Resonance*, 3rd ed.; Slichter, C. P., Ed.; Springer-Verlag: New York, 1990; Chapter 4.

(44) (a) Mulay, L. N. In *Theory and Applications of Molecular Paramagnetism*; Boudreaux E. A., Mulay, L. N., Eds.; John Wiley & Sons: New York, 1976; p 13. (b) Hattifield, W. E. *Ibid*.; Chapter 7, p 406. (c) Hattifield, W. E. *Ibid*.; p 382. (d) Mulay, L. N. *Ibid*.; p 17.

(45) (a) Jesson, J. P. In *NMR of Paramagnetic Molecules*; La Mar, G., Horrocks, W., Holm, R., Eds.; Academic: New York, 1973; Chapter 1. (b) Phillips, W. D. *Ibid*.; p 458.

(46) Reddy, B. V.; Khanna, S. N.; Dunlap, B. I. *Phys. Rev. Lett*. **1993**, *70*, 3323.

(47) Cox, A. J.; Louderback, J. G.; Bloomfield, L. A. *Phys. Rev. Lett*. **1993**, *71*, 923.

(48) Warren, W. W., Jr.; Norberg, R. E. *Phys. Rev*. **1967**, *154*, 277.

(49) Engelsberg, M.; Norberg, R. E. *Phys. Rev. B* **1972**, *5*, 3395.

(50) Andrew, E. R.; Eades, R. G. *Proc. R. Soc. London* **1953**, *A218*,

(51) Chang, T.-H.; Cheng, C.-P.; Yeh, C.-T. *J. Phys. Chem*. **1991**, *95*, 5239.

(52) Williams, E. D.; Thiel, P. A.; Weinberg, W. H.; Yates, J. T., Jr. *J. Chem. Phys*. **1980**, *72*, 3496.

(53) Hammer, L.; Heinz, K.; Muller, K. *Surf. Sci*. **1991**, *249*, 61.